Progress In Electromagnetics Research C, Vol. 134, 237–247, 2023

A Fourth-Order Bandpass Filter with High Selectivity and Out-of-Band Suppression

Ming-Ming Sun, Yun-Sheng Xu*, Qiao Zhang, Chang Chen, and Lingyun Zhou

Abstract—This paper presents a novel fourth-order bandpass filter with high selectivity and out-of-band suppression based on equivalent magnetic side wall cavities (MSWCs). By loading a via hole into an MSWC to produce a zero mode as a non-resonating node and using the dual MSWC modes TEM_{001} and TE_{100} as resonant modes, a modified doublet with two poles and two transmission zeros (TZs) can be formed. Three types of frequency response, either quasi-elliptic or asymmetric, can be obtained and designed flexibly. The TZs can be located on both sides of the passband or both on just one side. The mechanisms for generating the TZs are analyzed, and the adjustment of the TZ positions is discussed. The proposed four-pole quasi-elliptic filter with four TZs is a cascade of two such doublets with two different types of asymmetric response. It has been fabricated and measured to validate the design. Comparison is made with some previous work on substrate integrated waveguide filters. The developed filter is free from radiation and relatively compact among high order filters with multiple adjustable TZs based on cascaded cavities of the substrate integrated waveguide type.

1. INTRODUCTION

There has always been the pursuit of high performance in filter design, such as sharp selectivity, wide stopband with high rejection level, and compact size. To fulfill these requirements, one of the desires is that the filter has multiple transmission zeros (TZs) that can be flexibly adjusted in the design stage. Cross coupling is often utilized to generate additional TZs in filters based on substrate integrated waveguide (SIW) structures. This can be accomplished by multiple SIW cavities (SIWCs), e.g., three or four in [1, 2], to provide not only more transmission poles but also zeros. However, the filter size in this category is usually large. On the other hand, the filter structure is a combination of one dual- and a few single-mode SIWCs, so the number of controllable TZs that can be generated does not reach the maximum in view of the number of SIWCs used. More compact size with relatively more TZs can be realized by dual- and triple-mode designs. In [3–6], the fundamental or a higher order mode far from the passband of a dual-mode SIWC is employed as a non-resonating node (NRN) to provide an indirect source-load coupling. The corresponding coupling topology can be termed as a modified doublet [7], and two poles and up to two TZs can be generated. A fourth order filter with four TZs is obtained by a cascade of two such doublets. Since all the three modes concerned in a single doublet originate from merely one cavity of the SIW type, how to manage the TZs or to what extent each of them can be flexibly arranged is a remaining challenge for this kind of design. All the four TZs in the four-pole filter in [4] can be located in the upper stopband only, and then a third SIWC is added to design a five-pole quasi-elliptic filter with one and two TZs in the lower and upper stopbands, respectively. A complementary split ring resonator and quarter- and half-wavelength co-planar waveguide (CPW) resonators are etched on the top metallic surface of a square SIWC and half-mode SIWC (HMSIWC)

Received 2 May 2023, Accepted 21 June 2023, Scheduled 14 July 2023

* Corresponding author: Yun-Sheng Xu (xys@ustc.edu.cn).

The authors are with the Key Laboratory of Electromagnetic Space Information of the Chinese Academy of Sciences, Department of Electronic Engineering and Information Science, University of Science and Technology of China, Hefei, Anhui 230027, China.

in [8] and [9], respectively. Together with dual SIWC modes or the fundamental HMSIWC mode accordingly, an extended doublet [10] is realized and a third order filter with two TZs then designed. Filter design with mixed coupling mechanisms is also reported, using both planar waveguide or resonator and a SIWC mode as NRN. A third or fourth order filter with three TZs is proposed in [11–13] based on one SIWC only. However, the flexible design of the filter response with a single SIWC becomes increasingly difficult as the number of transmission poles and zeros grows.

In some of the above work, planar waveguides or resonators are introduced by etching on the top surface of a SIWC or HMSIWCs with some sides open to outside free space adopted to generate equivalent magnetic side walls. This destroys, however, the metallic shielding of the original closed SIWC and may cause radiation. In the substrate integrated folded waveguide technique, two layers of dielectric substrate are utilized, and an equivalent magnetic wall can be realized inside a closed cavity without any part of its outer surface open to outside free space [14, 15]. Due to the concept that the fundamental mode of a folded structure should resembles the field distribution of the TE_{101} mode in the original SIWC, however, magnetic side walls in a folded cavity are positioned where the original TE_{101} modal fields themselves show such performance, leading to a maximum of two magnetic walls. Recently, magnetic side wall cavity (MSWC) has been proposed, e.g., in [16]. It is a two-layered rectangular structure of the SIWC type and retains the shielding of the original SIWC. Modes with four equivalent magnetic side walls inside the cavity, called MSWC modes, can be obtained. A mode with significantly lower resonant frequency, namely zero mode [16, 17], can be further produced by the insertion of a via hole into the MSWC. The MSWC has been applied to the design of a second and third order filters in [18] and [19], respectively.

Based on two cascaded MSWCs, a compact fourth-order filter with four adjustable TZs is designed in this work. Each cavity is loaded with a via hole and performs a modified doublet function with two-poles and two TZs when being excited. MSWC modes TEM_{001} and TE_{100} are employed to form a passband, and the zero mode is as an NRN. To the authors' knowledge, this is the first time the zero mode is used as an NRN. Three different types of frequency response, either quasi-elliptic or asymmetric, can be obtained with a single doublet. Correspondingly, the two TZs are located on both sides of the passband or just on one side, and they can be flexibly adjusted, which are determined by the positions of the input and output ports and the inside via hole. The proposed four-pole filter is composed of two such doublets with two types of asymmetric filter response responsible for the lower and upper stopband performance, respectively. High selectivity and out-of-band rejection are achieved. The filter is free from radiation.

The filter structure and its design are presented in Section 2. In Section 3, the measurement results for the designed filter are given, and comparison is made with those obtained by simulation, as well as those in some previous work. Conclusions are drawn in Section 4.

2. STRUCTURE AND DESIGN

The proposed four-pole filter using double layers of dielectric substrate is depicted in Fig. 1. It is composed of two cascaded MSWCs, in either of which a via hole is embedded. Unless otherwise specified, the structural parameters in the remainder of the text are the same as those given in Fig. 1.

In the subsequent Section 2.1, eigenmode analysis is performed for a single MSWC loaded with a via hole. Then in Section 2.2, the coupling mechanisms for generating TZs and three types of frequency response under stripline excitation are discussed. The procedures for the design of the above fourth order filter with four TZs by cascading two such cavities are described in Section 2.3.

2.1. Eigenmode Analysis of a Single MSWC Inserted with a Via Hole

The MSWC in [16] is obtained by the insertion of a metallic patch between two layers of a dielectric substrate. The patch is surrounded by, but not connected with, via hole arrays, leaving a small gap in between in order to achieve four equivalent magnetic side walls located right at the edges of the patch and perpendicularly to the patch. The resonant frequency for the lowest order mode is decreased as compared to that for the conventional SIWC mode TE_{101}. The zero mode with even much lower eigenfrequency can be further produced by introducing a via hole into the cavity.

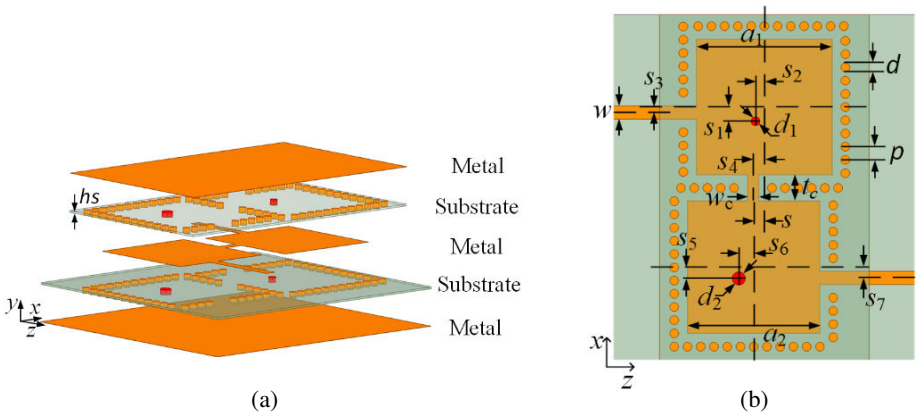

Figure 1. Structure of a four-pole filter. $a_1 = 15.35\,\text{mm}$, $a_2 = 15.0\,\text{mm}$, $w = 1.5\,\text{mm}$, $d_1 = 1.0\,\text{mm}$, $s_1 = 1.62\,\text{mm}$, $s_2 = 1.62\,\text{mm}$, $s_3 = 0.61\,\text{mm}$, $s_4 = 1.29\,\text{mm}$, $s = 1.20\,\text{mm}$, $w_c = 1.3\,\text{mm}$, $t_c = 1.5\,\text{mm}$, $d_2 = 1.5\,\text{mm}$, $s_5 = 1.26\,\text{mm}$, $s_6 = 1.69\,\text{mm}$, $s_7 = 1.20\,\text{mm}$, $d = 1.0\,\text{mm}$, $p = 1.5\,\text{mm}$. (a) 3D view. (b) Top view.

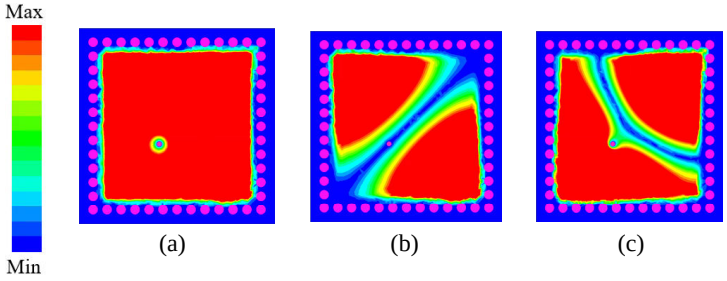

Figure 2. Field patterns for the first three modes in a MSWC inserted by a via hole. $a_1 = 15$, $d_1 = 0.5\,\text{mm}$, $s_1 = s_2 = 1.9\,\text{mm}$. (a) Zero mode, 2.28 GHz. (b) MSWC Mode I, 5.07 GHz. (c) MSWC Mode II, 5.16 GHz.

The field patterns for the first three modes in a single MSWC with a via hole inside are illustrated in Fig. 2. As eigenmode solutions, conventional SIWC modes resonant at higher frequencies are also available. The structure is geometrically symmetric in the y-direction perpendicular to the patch; therefore, the SIWC modes, all with antisymmetric field distributions, cannot be excited with stripline input and output in the patch plane as shown Fig. 1.

For a square patch as in Fig. 2, the MSWC modes TEM_{001} and TE_{100} are degenerate and orthogonal. Any of their linear combinations are eigenmodes as well. Orthogonal MSWC Modes I and II are exactly two such situations. Perturbed by the inside via hole, they become nondegenerate. Modes I and II are to be employed as working modes to comprise a passband.

The zero mode becomes now the lowest order mode. It is well known in microstrip patch antenna design [17]. Recently, it has been found in [16] that such a mode may also exist in a closed MSWC. In fact, among all the rectangular SIWCs with six possible combinations of electric and magnetic side walls, only the MSWC type may produce that mode through the insertion of a via hole. Although the zero mode is extra generated and does not belong to the eigemmode spectrum of a standard MSWC, it behaves like an MSWC mode in the sense that four equivalent magnetic side walls are also available exactly at the same places. It is intended to be used as an NRN to help produce an additional TZ.

When an eigenmode is utilized as an NRN, its resonance is required to be at a frequency far from the passband so as to avoid possible significant deterioration of filter performance, especially outside of the passband. As can be seen from Fig. 2, the zero mode has a substantially lower frequency. In fact, the frequency separation is larger than that can be realized by its counterparts in previous work. A further requirement is that near or not far from the passband the field of the zero mode should be

strong enough so that its bypass coupling may bring about a TZ. First, as the lowest order mode it is usually easier to be exited than higher order modes. Second, its field distribution is nearly uniform except in the vicinity of the inside via hole, as illustrated in Fig. 2(a), so its excitation is not sensitive to the input and output port positions. This feature is unique and not available to the other modes, which also simplifies the design and allows more flexible adjustment of the coupling that leads to TZs.

2.2. Frequency Response of an Excited MSWC Inserted with a via Hole

When the preceding MSWC is excited by striplines as illustrated in Fig. 3, a modified doublet [7] is achieved with two poles and two TZs. Three types of frequency response are available, as shown in Fig. 4. The diversity is mainly due to different choices for the positions of the feeding ports and the via hole. Changing the diameter d_1 of the via hole may also make a difference, though less significant. The concrete parameters with which the simulation results in Fig. 4 are obtained are given in Table 1. For Type A to C, the via hole is located in the lower right, lower left, and upper right quarter regions, respectively. The two TZs can be located on both sides of the passband or only on one side as in [3].

Table 1. Geometrical parameters generating three types of response.

Type	a	w	s_1	s_2	s_3	s_4	d_1	Zero Mode (GHz)	Mode I (GHz)	Mode II (GHz)
A	15.0	1.5	1.35	−1.35	0.2	0.2	0.8	2.52	5.31	5.09
B	15.0	1.5	1.9	1.9	1.0	1.0	0.5	2.28	5.07	5.44
C	15.0	1.5	−0.84	−0.84	−0.7	−0.7	0.6	2.43	5.07	5.16

(Dimension in millimeters)

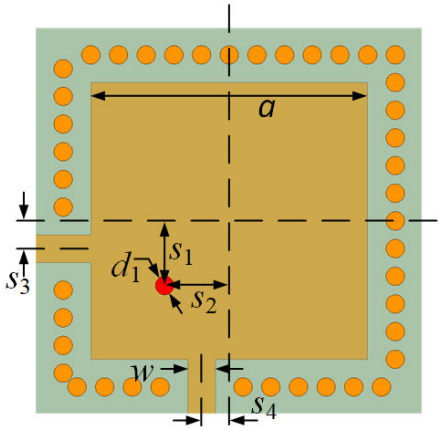

Figure 3. Structure of an excited MSWC with a via hole inside.

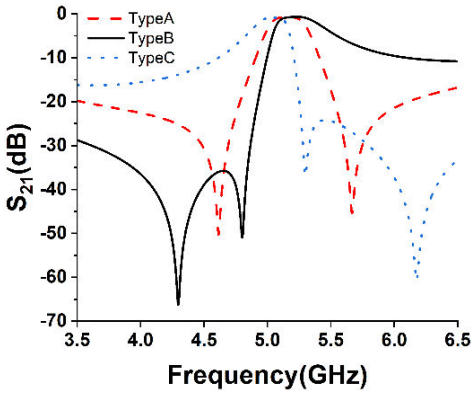

Figure 4. Three different types of response for the MSWC loaded with a via hole.

It is seen from Figs. 2 and 3 that the electric fields for Mode I at input and output ports are out of phase, whereas they are in phase for Mode II. If the signal amplitudes of these two working modes are the same or nearly so, a TZ, called intrinsic TZ, can be generated. It is normally near the passband. The corresponding coupling matrix can be written as:

$$\mathrm{m} = \begin{bmatrix} 0 & m_{S1} & m_{S2} & m_{SL} \\ m_{S1} & m_{11} & 0 & m_{L1} \\ m_{S2} & 0 & m_{22} & m_{L2} \\ m_{SL} & m_{L1} & m_{L2} & 0 \end{bmatrix}, \tag{1}$$

where $m_{S1} = -m_{L1}$ and $m_{S2} = m_{L2}$ due to the above mentioned odd and even mode characteristics, respectively. Only two modes are concerned here, and the direct coupling between the source and load m_{SL} is zero. In this case, the expression for the TZ position can be derived rigorously [20], and the normalized frequency Ω_{TZ} of lowpass prototype is given by

$$\Omega_{\mathrm{TZ}} = -m_{11} - \frac{m_{S1}m_{L1}(m_{22} - m_{11})}{m_{S1}m_{L1} + m_{S2}m_{L2}} = \frac{m_{11}m_{S2}^2 - m_{22}m_{S1}^2}{m_{S1}^2 - m_{S2}^2}, \tag{2}$$

For negative or positive Ω_{TZ}, the TZ is in the lower or upper stopband, respectively. Since the center frequency (CF) of the passband lies between the resonant frequencies of the Modes I and II, m_{11} and m_{22} have opposite signs. Therefore, the position of the intrinsic TZ can be one of the following four cases: 1) when $m_{11} < 0$, $m_{22} > 0$, $|m_{S1}| > |m_{S2}|$, in the lower stopband; 2) when $m_{11} < 0$, $m_{22} > 0$, $|m_{S1}| < |m_{S2}|$, in the upper stopband; 3) when $m_{11} > 0$, $m_{22} < 0$, $|m_{S1}| > |m_{S2}|$, in the upper stopband; 4) when $m_{11} > 0$, $m_{22} < 0$, $|m_{S1}| < |m_{S2}|$, in the lower stopband.

An additional TZ can be produced by cross-coupling, and the corresponding topology is demonstrated in Fig. 5. The input and output striplines located inside the cavity are connected with microstrip lines immediately outside the cavity. This kind of connection provides an inductive coupling, and the coupling coefficient is negative, leading to a phase shift about $-90°$. Since the passband is above the resonant frequency of the zero mode, the phase shift due to the zero mode is also about $-90°$. The total phase shift from source to load for the NRN signal path is approximately $-270°$, which is equivalent to a capacitive coupling, and the coupling coefficient is positive. Therefore, the initial topology of Fig. 5(a) can be equivalent to Fig. 5(b). The zero mode provides a secondary coupling path from source to load. Either the interaction between the odd-mode and the secondary paths or that between the even mode and the secondary paths will cause a TZ. Proper phase relation is not the only condition for the generation of a TZ. The signal amplitudes between two paths are also required to be approximately equal. In practice, merely one such TZ is obtained.

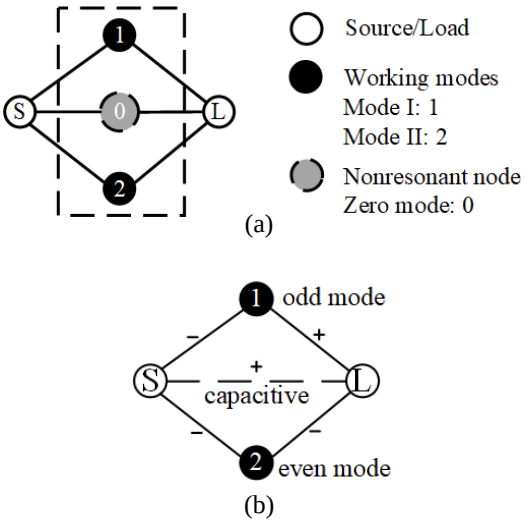

Figure 5. Topology of the cross-coupling. (a) Initial topology. (b) Equivalent topology.

One can still use a coupling matrix of order 4×4 to explain the generation of both TZs together as in [7]. It is formally the same as (1). In order to take into account the effect of the zero mode, however, m_{SL} cannot be zero anymore, and it is positive as discussed above. Alternatively, one can employ a 5×5 coupling matrix similar to (1) in which the couplings with the zero mode are explicitly shown as with the other two modes. The order of the concerned nodes is the source, the zero mode, Mode I, Mode II, and the load. In this case, m_{SL} is zero.

The locations of these two TZs can be adjusted in the way described previously in obtaining three different types of frequency response as in Fig. 4. The coupling coefficients m_{Si} and m_{Li} can be extracted as in [21] and the diagonal elements calculated as in [3].

As examples, the comparison of S-parameters for Types B and C responses, computed by simulation software and the extracted coupling matrix, respectively, is shown in Fig. 6. One TZ is intrinsic, and the other is produced by cross-coupling. For Type B in Fig. 6(a), the self-coupling coefficients of the odd and even modes are positive and negative, respectively, and the coupling coefficient between the former and source is smaller than that between the latter and source. This corresponds to the aforementioned fourth case regarding the position of the intrinsic TZ. Therefore, the TZ near the passband is intrinsic. And the intrinsic TZ near the passband belongs to the third case for Type C in Fig. 6(b).

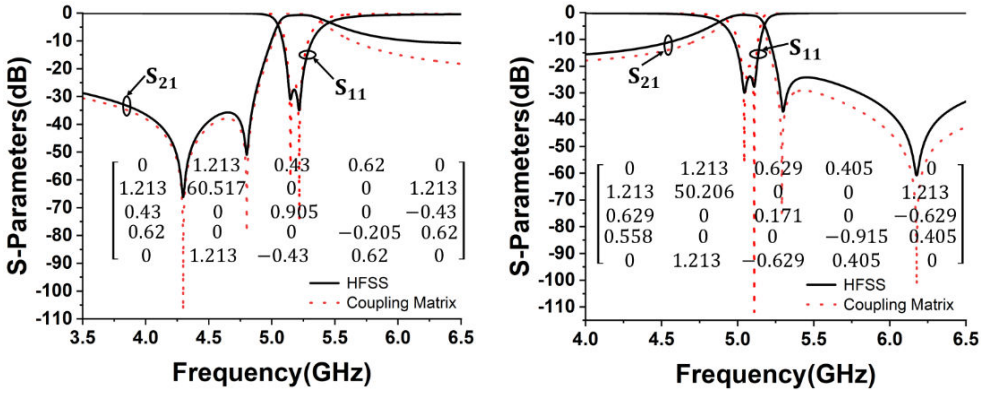

Figure 6. Simulated responses and extracted coupling matrix. (a) Type B. (b) Type C.

2.3. Design of the Proposed Four-Pole Filter

In previous dual-cavity filter design, single-cavities with quasi-elliptic response are often chosen for cascade. In this work, the range of flexible adjustment for a doublet with a Type A response is relatively small, thus the four-pole filter is composed of two doublets with different types of asymmetric response, namely Types B and C. The first step is to design a single cavity and figure out the trend in the changing of each TZ with the via hole and port positions, so as to provide a guide to the further design of the dual-cavity filter. The initial geometrical parameters of the single-cavity in Fig. 3 can be determined by design specification. The resonant frequency f of the degenerate Modes I and II, namely two linear combinations of the TEM_{001} and TE_{100} MSWC modes, is given by [16]

$$f = \frac{c}{2a\sqrt{\mu_r \varepsilon_r}} \tag{3}$$

where c is the velocity of light, and μ_r and ε_r are the relative permeability and permittivity of the medium, respectively. The choice of the patch size $a \times a$ should make f somewhat lower than the desired CF, because at least the resonant frequency of one of the initially degenerate modes will increase after loading the via hole. The analytical estimation of the resonant frequency of the zero mode can be obtained according to the theory in [17].

The simulated $|S_{21}|$ of Types B and C responses along with different s_3 and s_1 are shown in Figs. 7 and 8, respectively. For Type B, the two TZs move apart as s_3 increases, whereas they become closer to each other for larger s_1. For Type C, the cross-coupling TZ shifts to a higher frequency with increasing s_3; however, the intrinsic TZ is not much influenced. A reverse situation can be observed for larger s_1. The bandwidth can also be tuned through the via hole.

Cascading Type B and Type C results in the dual-cavity filter depicted in Fig. 1, with two TZs on each side of the passband. The first and second cavities are responsible for lower and upper stopband performances, respectively. Adjusting the TZs in the cascaded structure with the above geometrical parameters is similar and thus not shown here, which also means that the lower and upper stopband performance can be independently tuned with these parameters. For more design freedom, s_4 and s_3 or s_2 and s_1 do not have to be equal.

The influence of the coupling stripline between the cavities is illustrated in Fig. 9. It may also affect the positions of the TZs.

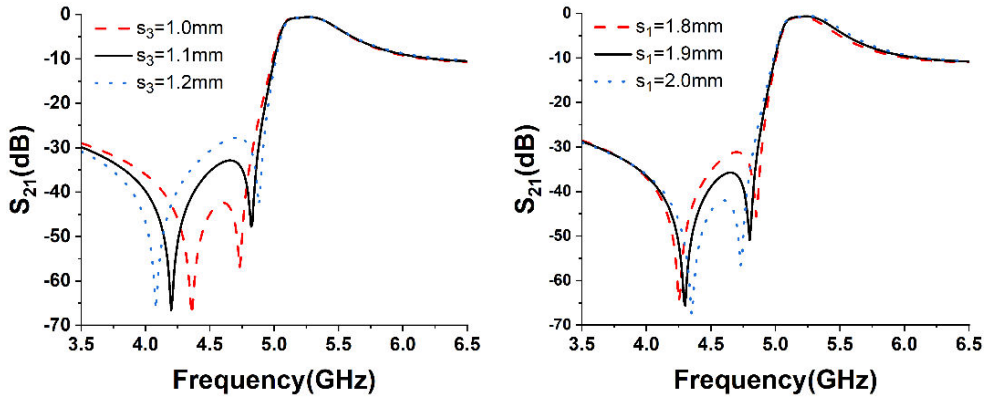

Figure 7. Frequency response of Type B adjusted by s_3 and s_1. (a) $s_4 = s_3$. (b) $s_2 = s_1$.

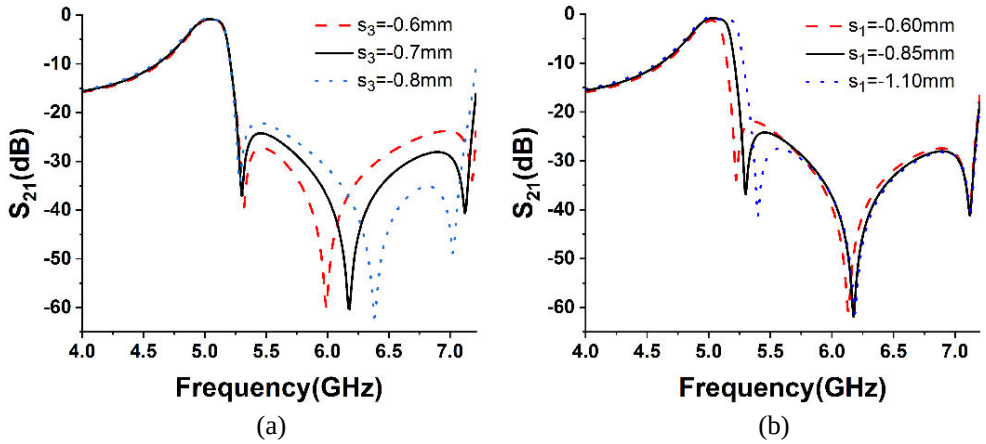

Figure 8. Frequency response of Type C adjusted by s_3 and s_1. (a) $s_4 = s_3$. (b) $s_2 = s_1$.

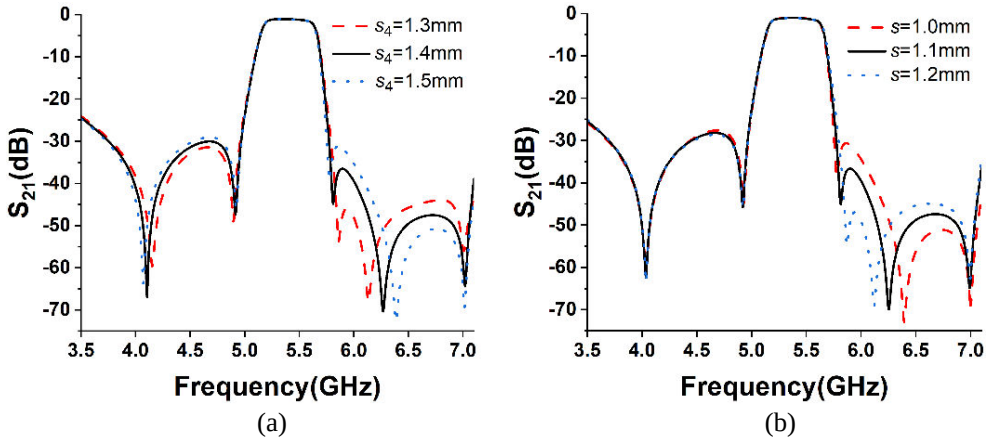

Figure 9. Frequency response adjustment of the proposed filter. (a) By s_4. (b) By s.

3. EXPERIMENT

The designed dual-cavity filter is fabricated by the printed circuit board technology and its performance measured. Rogers' RO4350B with a thickness of 0.508 mm, dielectric constant of 3.66, and loss tangent of 0.004 is used as substrate and RO4450F with a thickness of 0.101 mm as prepreg to glue the substrates. The other structural parameters are given in Fig. 1. The measured and simulated S-parameters are illustrated in Fig. 10. There are four poles and five TZs. The highest TZ is due to interaction of higher order modes [19] and cannot be designed using the method in Section 2. The measured CF f_0 is 5.32 GHz, and the fractional bandwidth (FBW) is 9.0%. The minimum in-band insertion loss (IL) is 2.26 dB and the return loss larger than 15.4 dB. The out-of-band suppression above the passband is larger than 44 dB from $1.08f_0$ to $1.32f_0$ and that below 30 dB from $0.70f_0$ to $0.92f_0$. The filter size is $0.69\lambda \times 1.27\lambda$, where λ is the wavelength in the dielectric substrates at the CF. It is relatively compact among high order filters with multiple adjustable TZs based on cascaded SIW type cavities.

The measured S-parameters shift slightly to the lower frequency band relative to the simulation ones, and the IL increases, which may be caused by simulation errors and fabrication tolerance. The model for the prepreg in the simulation also deviates from its practical situation in the fabrication process. In general, the measured and simulated results are in good agreement.

Table 2. Comparison with some previous work.

Ref.	Resonator	f_0 (GHz)	FBW (%)	IL (dB)	Np	Nz	Lower Stopband	Upper Stopband	Size (λ^2)
[1]-III	SIW	12.46	3.7	1.36	4	3	NA	NA $\sim 1.27f_0$ (> 40 dB)	2.77
[1]-IV	SIW	12.47	3.7	1.89	4	3	NA	NA $\sim 1.28f_0$ (> 20 dB)	2.77
[3]	SIW	15	4.3	1.7	4	5	$0.73 \sim 0.96f_0$ (> 46 dB)	$1.05 \sim 1.28f_0$ (> 48 dB)	3.25
[4]-I	SIW	10	3.3	1.55	4	4	NA	$1.03f_0 \sim$ NA (> 30 dB)	2.0
[4]-II	SIW	10	3.5	2.04	5	3	NA $\sim 0.96f_0$ (> 30 dB)	$1.03f_0 \sim$ NA (> 30 dB)	3.77
[5]	HMSIW	10	5.3	2.40	4	4	NA $\sim 0.92f_0$ (> 30 dB)	$1.05f_0 \sim$ NA (> 30 dB)	1.75
[12]-I	SIW + UIR	9.99	6.2	1.18	3	4	$0.67 \sim 0.95f_0$ (> 28.5 dB)	$1.10 \sim 1.27f_0$ (> 25 dB)	1.44
[12]-II	SIW + UIR	9.93	8.4	1.19	3	3	$0.69 \sim 0.89f_0$ (> 25 dB)	$1.06 \sim 1.30f_0$ (> 29 dB)	1.42
[22]	QMSIW + EMSIW	8.0	11	0.9	3	3	NA	$1.10 \sim 1.96f_0$ (> 23 dB)	0.32
[23]	QWSIW	5	11.3	1.85	4	5	NA	NA $\sim 1.93f_0$ (> 20 dB)	0.52
[24]	QMSIW + CRLH TL	8.4	14.3	1.55	4	3	NA	NA $\sim 1.85f_0$ (> 20 dB)	0.28
[25]	QMSIW	30	20	2.85	4	4	NA	NA $\sim 3.6f_0$ (> 26 dB)	0.59
This Work	MSWC	5.32	9.0	2.26	4	5	$0.70 \sim 0.92f_0$ (> 30 dB)	$1.08 \sim 1.32f_0$ (> 44 dB)	0.88

Np: Number of poles; Nz: Number of TZs; NA: Not available in the reference.

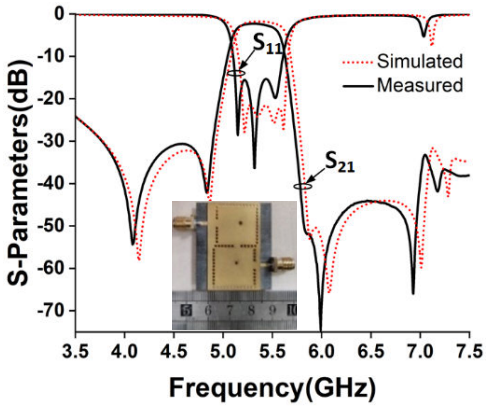

Figure 10. Simulated and measured results for the four-pole filter.

Performance comparison with some single passband filters in previous work with at least three poles and three TZs is presented in Table 2.

The in-band IL in the present filter is not so small. The reason is the use of substrates with larger loss tangent as in [16], among others. For a single MSWC as in Fig. 3, the unloaded quality factors for the TEM_{001} and TE_{100} modes are both about 148 with a square patch of $15.0 \times 15.0\,mm^2$ and without the inside via hole. The other work referred to in Table 2 except [24, 25] employs substrates with a thickness of 0.508 mm, dielectric constant of 2.2, and loss tangent of 0.0009. If such substrates are used instead, the unloaded quality factors for the above two modes are 276–277 with a larger patch size of $19.55 \times 19.55\,mm^2$ to ensure nearly the same resonant frequencies. The loss tangents are 0.001 and 0.0008 in [24] and [25], respectively.

4. CONCLUSION

A novel four-pole bandpass filter is designed based on MSWCs. A via hole is inserted inside each cavity. The generated zero mode with significantly lower resonant frequency is used as an NRN. The building block for the design is a modified doublet obtained with dual-modes of the MSWC and the NRN. It may provide three types of frequency response, quasi-elliptic or asymmetric, with two poles and two zeros. The TZs can be flexibly adjusted on both sides of the passband or just on one side. The proposed filter with four adjustable TZs is a cascade of two such doublets with different types of asymmetric response. The filter is of compact size and radiation free due to equivalent magnetic side walls located inside a shielded structure. The measured results agree well with simulated ones. High selectivity and out-of-band rejection level are achieved as expected.

REFERENCES

1. Liu, Q., D. Zhou, Y. Zhang, D. Zhang, and D. Lv, "Substrate integrated waveguide bandpass filters in box-like topology with bypass and direct couplings in diagonal cross-coupling path," *IEEE Trans. Microw. Theory Techn.*, Vol. 67, No. 3, 1014–1022, Mar. 2019.
2. Zhu, F., W. Hong, J. -X. Chen, and K. Wu, "Cross-coupled substrate integrated waveguide filters with improved stopband performance," *IEEE Microw. Wireless Compon. Lett.*, Vol. 22, No. 12, 633–635, Dec. 2012.
3. Chu, P., W. Hong, M. Tuo, K.-L. Zheng, W.-W. Yang, F. Xu, and K. Wu, "Dual-mode substrate integrated waveguide filter with flexible response," *IEEE Trans. Microw. Theory Techn.*, Vol. 65, No. 3, 824–830, Mar. 2017.
4. Zhu, F., G. Q. Luo, B. You, X. H. Zhang, and K. Wu, "Planar dual-mode bandpass filters using perturbed substrate-integrated waveguide rectangular cavities," *IEEE Trans. Microw. Theory Techn.*, Vol. 69, No. 6, 3048–3057, Jun. 2021.

5. Zhu, F., G. Q. Luo, Z. Liao, X. W. Dai, and K. Wu, "Compact dual-mode bandpass filters based on half-mode substrate-integrated waveguide cavities," *IEEE Microw. Wireless Compon. Lett.*, Vol. 31, No. 5, 441–444, May 2021.
6. Liu, Q., D. Zhou, S. Wang, and Y. Zhang, "Highly-selective pseudoelliptic filters based on dual-mode substrate integrated waveguide resonators," *Electron. Lett.*, Vol. 52, No. 14, 1233–1235, Jul. 2016.
7. Amari, S. and U. Rosenberg, "A universal building block for advanced modular design of microwave filters," *IEEE Microw. Wireless Compon. Lett.*, Vol. 13, No. 12, 541–543, Dec. 2003.
8. Wu, L.-S., X.-L. Zhou, Q.-F. Wei, and W.-Y. Yin, "An extended doublet substrate integrated waveguide (SIW) bandpass filter with a complementary split ring resonator (CSRR)," *IEEE Microw. Wireless Compon. Lett.*, Vol. 19, No. 12, 777–779, Dec. 2009.
9. Shen, W., "Extended-doublet half-mode substrate integrated waveguide bandpass filter with wide stopband," *IEEE Microw. Wireless Compon. Lett.*, Vol. 28, No. 4, 305–307, Apr. 2018.
10. Amari, S. and U. Rosenberg, "New building blocks for modular design of elliptic and self-equalized filters," *IEEE Trans. Microw. Theory Techn.*, Vol. 52, No. 2, 721–736, Feb. 2004.
11. Liu, Z., G. Xiao, and L. Zhu, "Triple-mode bandpass filters on CSRR-loaded substrate integrated waveguide cavities," *IEEE Trans. Compon., Packag. Manuf. Technol.*, Vol. 6, No. 7, 1099–1105, Jul. 2016.
12. Zhu, Y. and Y. Dong, "UIR-loaded dual-mode SIW filter with compact size and controllable transmission zeros," *2020 IEEE/MTT-S International Microwave Symposium (IMS)*, 667–670, Los Angeles, CA, USA, Aug. 2020.
13. Liu, Q., D. Zhou, D. Lv, D. Zhang, and Y. Zhang, "Ultra-compact highly selective quasi-elliptic filters based on combining dual-mode SIW and coplanar waveguides in a single cavity," *IET Microw. Antennas Propag.*, Vol. 12, No. 3, 360–366, Feb. 2018.
14. Alotaibi, S. K. and J.-S. Hong, "Novel substrate integrated folded waveguide filter," *Microw. Opt. Technol. Lett.*, Vol. 50, No. 4, 1111–1114, Apr. 2008.
15. Moro, R., S. Moscato, M. Bozzi, and L. Perregrini, "Substrate integrated folded waveguide filter with out-of-band rejection controlled by resonant-mode suppression," *IEEE Microw. Wireless Compon. Lett.*, Vol. 25, No. 4, 214–216, Apr. 2015.
16. Ji, Q., Y.-S. Xu, C. Chen, L. Zhou, and Y.-F. Zhang, "Cavities with four equivalent magnetic side walls in composite planar multilayered and substrate integrated waveguide structures," *2020 International Conference on Microwave and Millimeter Wave Technology (ICMMT)*, Shanghai, China, Sept. 2020.
17. Porath, R., "Theory of miniaturized shorting-post microstrip antennas," *IEEE Trans. Antennas Propag.*, Vol. 48, No. 1, 41–47, Jan. 2000.
18. Sun, M.-M., Y.-S. Xu, C. Chen, and L. Zhou, "A compact bandpass filter with high selectivity and wide stopband," *2023 International Conference on Microwave and Millimeter Wave Technology (ICMMT)*, Qingdao, China, May 2023.
19. Zhang, Y.-F., Y.-S. Xu, C. Chen, and L. Zhou, "Miniaturized single band filter with wide outer-band rejection at higher frequencies," *2021 Photonics & Electromagnetics Research Symposium (PIERS)*, 1520–1526, Hangzhou, China, Nov. 21–25, 2021.
20. Amari, S. and U. Rosenberg, "Characteristics of cross (bypass) coupling through higher/lower order modes and their applications in elliptic filter design," *IEEE Trans. Microw. Theory Techn.*, Vol. 53, No. 10, 3135–3141, Oct. 2005.
21. Hong, J.-S., *Microstrip Filters for RF/Microwave Applications*, 2nd Edition, John Wiley & Sons Inc., Hoboken, NJ, USA, 2011.
22. Kim, P. and Y. Jeong, "Compact and wide stopband substrate integrated waveguide bandpass filter using mixed quarter- and one-eighth modes cavities," *IEEE Microw. Wireless Compon. Lett.*, Vol. 30, No. 1, 16–19, Jan. 2020.
23. Shi, Y., K. Zhou, C. Zhou, and W. Wu, "Compact QMSIW quasi-elliptic filter based on a novel electric coupling structure," *Electron. Lett.*, Vol. 53, No. 23, 1528–1530, Nov. 2017.

24. Pelluri, S. and M. V. Kartikeyan, "Compact QMSIW bandpass filter using composite right/left-handed transmission line in grounded coplanar waveguide," *Int. J. RF Microw. Comput.-Aided Eng.*, Vol. 28, No. 9, Nov. 2018.
25. Huang, X.-L., L. Zhou, M. Völkel, A. Hagelauer, J.-F. Mao, and R. Weigel, "Design of a novel quarter-mode substrate-integrated waveguide filter with multiple transmission zeros and higher mode suppressions," *IEEE Trans. Microw. Theory Techn.*, Vol. 66, No. 12, 5573–5584, Dec. 2018.